

Moving Beyond the Finite Elements, a Comparison Between the Finite Element Methods and Meshless Methods for a Ballistic Impact Simulation

Murat Buyuk, Cing-Dao Steve Kan, Nabih E. Bedewi

FHWA/NHTSA-NCAC, National Crash Analysis Center, The George Washington University

Ali Durmus, Sedat Ulku

Uludag University, Faculty of Engineering and Architecture, Dept. of Mechanical Engineering

Abstract

For the past several decades, finite element techniques have been used extensively for the analysis of computational solid mechanics problems. However, when the distortions become very severe, especially Lagrangian finite element algorithms are not always adequate. More recently meshless methods (or particle methods) have been developed and applied to solid mechanics problems since they can efficiently be used to represent severe distortions and are more robust for dynamics problems such as high energy impacts and penetrations that involve large deformations and even erosions. Impacts at higher speeds are also challenging because of the high strain rate behavior of the materials and the significant importance of the stress wave propagation through the material. In this paper, the deformation pattern and characteristics of a thin (50 μm) foil is investigated both numerically and experimentally under impact loading of a 9 mm standard NATO bullet, at several speeds by using a 3D non-linear explicit numerical code, LS-DYNA. Different element and particle algorithms are used to obtain the best numerical representation of the problem. The differences between Lagrangian, Eulerian, ALE (Arbitrary Lagrangian-Eulerian) and SPH (Smoothed Particle Hydrodynamics) formulations are briefly compared and discussed under ballistic impact conditions. The results obtained from these different numerical models are also validated with a series of tests and are in good agreement with the experimentally measured values.

Keywords: *Ballistic Impact, Penetration, Meshless Methods*

Introduction

Accurate and realistic simulation of problems involving high-velocity impact and penetration, in applications such as ballistic penetration presents a variety of challenges. These problems typically involve large deformations, even erosions, nonlinear strain rate and shock wave dependent material behaviors [1].

In terminal ballistics, determining the ballistic performance of a projectile or armor requires the usage of some sophisticated techniques. Usually experimental studies are performed to find the ballistic limit of the system. Measuring the initial and residual velocity is one of the criteria needed to determine the ballistic performance. For this purpose several methods are successfully implemented and used in the literature. In this paper, behavior of a very thin (50 μm) copper foil

that is used in an experimental set-up designed to measure the projectile velocity, is investigated both experimentally and numerically under ballistic impact.

In a numerical model of a continuum, the material is discretised into finite sections over which, the conservation and constitutive equations are solved. The way in which this spatial discretisation is performed leads to different numerical methods [2]. For problems such as ballistic impact, there typically is no single best numerical method which is applicable to all parts of a problem. Techniques to couple different types of numerical solvers in a single simulation can allow the use of the most appropriate solver for each domain of the problem. In the numerical part of the study, different element and particle algorithms are used to discretise the continuum provided by LS-DYNA, which is a non-linear explicit dynamics code. The methods used in this study are: Lagrangian, Eulerian, ALE (Arbitrary Lagrangian-Eulerian) and SPH (Smoothed Particle Hydrodynamics). The differences between these numerical schemes under the effect and challenges of simulating ballistic impact are then compared.

Numerical Solvers

Different numerical solvers provided by LS-DYNA and their properties are summarized below as follows:

Lagrangian

In the Lagrangian solver, the numerical mesh moves and distorts with the physical material as shown in Figure 1. This formulation is widely used because of its advantages, such as being able to track accurately and efficiently material interfaces and incorporate complex material models. This formulation is generally used to represent solid materials however, is very sensitive to distortions resulting small time step and possible loss of accuracy. Very well known negative-volume error occurs as a result of this mesh tangling. Numerical codes can handle these problems with adaptivity or re-meshing algorithms or by eroding the highly distorted elements by using usually a plastic strain threshold value. Adaptivity and re-meshing can be computationally costly and even not possible in some 3-D cases. Besides, element erosion algorithms can cause loss of accuracy since it removes the strain energy from the calculation. Also the amount of mass lost, affects the inertial properties of the model. Some problems may also occur if erosion happens at the contact interface where, a contact-impact algorithm is used [3].

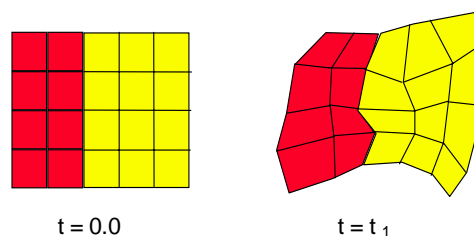


Figure 1. Lagrangian Finite Element Mesh

Eulerian

In the Eulerian solver, the numerical mesh is fixed in space and the physical material flows through the mesh as shown in Figure 2. This formulation is generally used to represent fluids and gases, usually for flow problems that even involve multi-material properties within one finite element cell. Free surfaces and material interfaces can move through the fixed mesh, which also brings a need to model a void mesh. Large deformations do not result in mesh distortions. However, extra computational time required to maintain interfaces and to limit numerical diffusion. Also, to describe solid behavior, the solid stress tensor and the history of the material must also be transported from cell to cell.

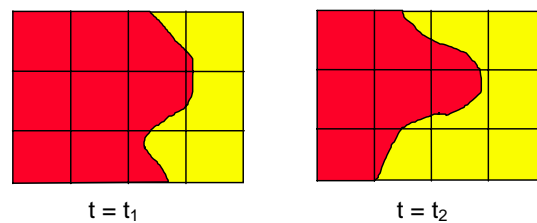


Figure 2. Eulerian Finite Element Mesh

Arbitrary Lagrangian Eulerian (ALE)

In the ALE solver, solver allows for a type of "automatic rezoning", which can be quite useful for certain problems. Depending on the specified motions, the ALE domain can be completely Lagrangian (the nodes move with the material motion), completely Eulerian (the nodes are fixed and the material moves through the fixed mesh), or something in between as shown in Figure 3. ALE may be used for the modeling of solids, fluids, and gases. It is particularly well suited for a variety of fluid-structure interaction problems. In a single material ALE solver the primary assumption is that all nodes at free boundaries or at material interfaces are strictly Lagrangian. Thus, no material may flow in or out of ALE domain, nor may individual cells contain more than one material. Multiple material ALE formulations do not have such restrictions and can operate in the same fashion as multiple material Euler schemes wherein material may flow from cell to cell.

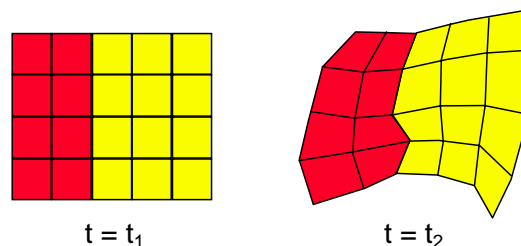


Figure 3. ALE Finite Element Mesh

Smoothed Particle Hydrodynamics (SPH)

One of the meshless techniques that LS-DYNA providing is the SPH method, where the other one is the Element Free Galerkin (EFG) method. SPH is a Lagrangian technique developed initially to simulate astrophysical problems having the potential to be efficient and accurate at

modeling material deformation as well as flexible in terms of the inclusion of specific material models. In addition, SPH is a meshless or gridless technique such that it does not suffer from the normal problems of grid tangling in large deformation problems. Presently many large deformation problems are calculated using Eulerian techniques that do not suffer from grid tangling but have some limitations in terms of modeling material interfaces, the inclusion of specific material models, and associated high computational expense. The main potential advantages of the SPH technique are that in not requiring a numerical grid, no grid tangling. SPH is Lagrangian in nature thus allowing efficient tracking of material deformations and history dependent behavior. Compared with Euler, it is more efficient in that one only need model regions where materials exist, not all regions where material might exist as a void. Being meshless, phenomenon such as fracture and fragmentation may be modeled. Fracture can occur arbitrarily without the a priori strictures of a numerical mesh. With all of its promise, however, SPH technology is relatively immature compared with standard grid based Lagrangian and Eulerian techniques. Several problems need to be solved before the technique becomes a fully developed computational continuum dynamics technique. There are remaining known problems in the areas of stability, consistency, and conservation. The SPH particles describe the Lagrangian motion of mass points that are really interpolation points as shown in Figure 4. Particles are approximated by a cubic B-spline function.

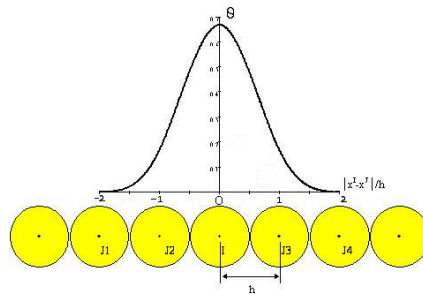


Figure 4. SPH Interpolation Points

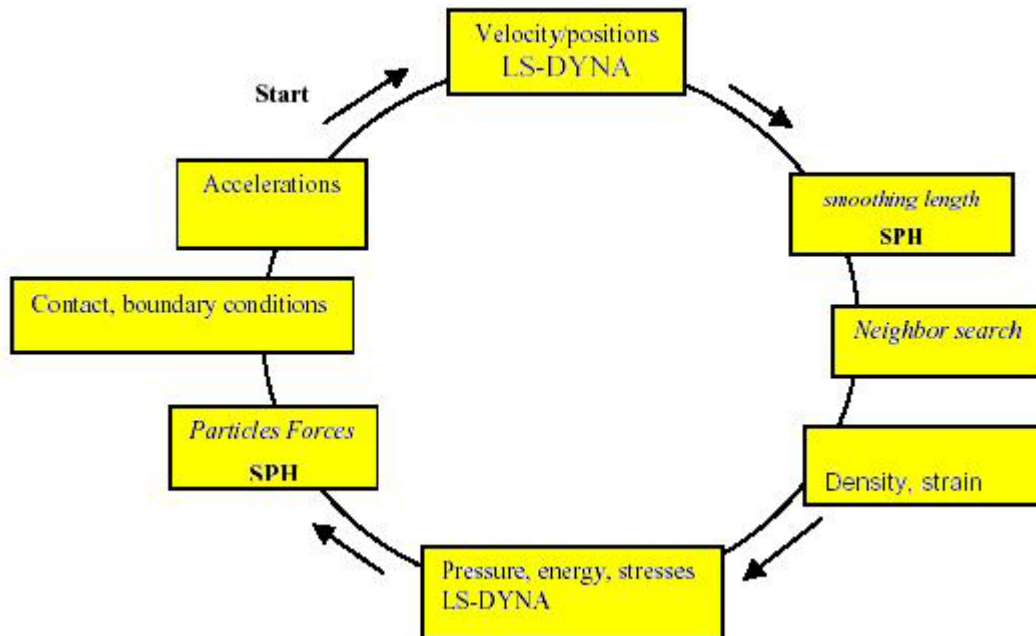


Figure 5. LS-DYNA Explicit Scheme for SPH Calculation

Experimental Set-Up

An experimental set-up is designed to measure the velocity of several bullets some of which were belong to 9 x 19 mm standard NATO Cartridges (Figure 6) that are manufactured by Makine ve Kimya Endüstrisi (MKE) Kurumu Gazi Fişek Fabrikası (Ankara/TÜRKİYE). These cartridges contained different amounts of Ball Powder[®] gunpowder changing between 380mg to 38mg to obtain different impact velocities.



Figure 6. 9 x 19 mm Standard NATO Bullet

The barrel used during the experimental study and the experimental set-up is shown in Figure 7 and 8 respectively. The measured velocities were between 69 m/s and 377 m/s for the cartridges. In addition, the 50 μ m thick copper foils were analyzed as a function of their damage geometry as they were in use during the measurements of velocities.

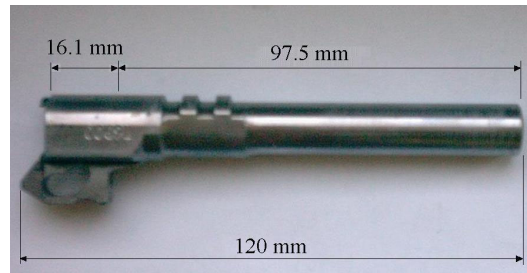


Figure 7. Barrel



Figure 8. Experimental Set-Up

Numerical Modeling Methodology

To understand the differences in behavior of foil when different element formulations are used, the impacting bullet is modeled by finite elements where Lagrangian formulation is used to satisfy the consistency between the models. So, the numerical models are also representing a coupling between a Lagrangian finite element mesh and the before mentioned algorithms. The models are coupled by contact-impact algorithms.

Geometric Model

Since, the effect of both shell and solid elements are also investigated, two different models are used to be able to mesh the structures with the corresponding elements. For the shell elements the target model consists of one planer surface, which is modeled as circular to avoid the unwanted effect of reflecting shock wave. This model also consists of three concentric layers, where the inner most layers are meshed finer than the surrounding other two layers for accuracy and contact related concerns. The target geometric model is represented in Figure 9. For the hexahedral solid elements the same pattern preserved for a volumetric cylindrical model.

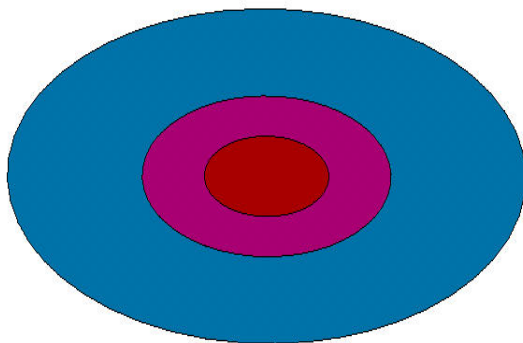


Figure 9. Target Geometry

The impacting bullet is modeled to be able to map-mesh it with hexahedral solid elements. The exact geometry of the standard 9 x 19 mm NATO bullet is preserved for this purpose and the bullet jacket and the core is also modeled and meshed separately. A contact interface is used between the core and the jacket. The geometric dimensions of the bullet are shown in Figure 10. The CAD model of the bullet is represented in Figure 11.

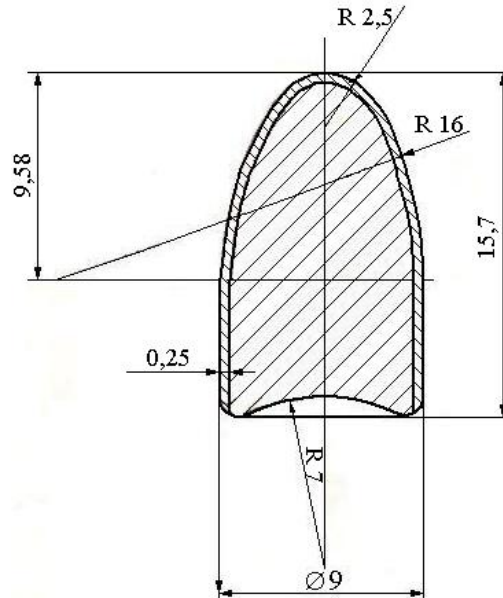
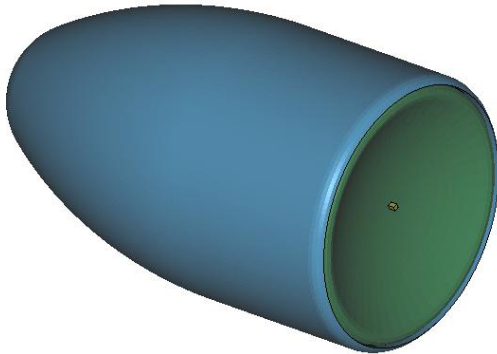
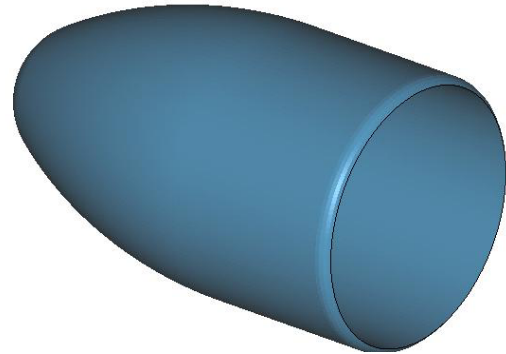


Figure 10. Bullet Dimensions

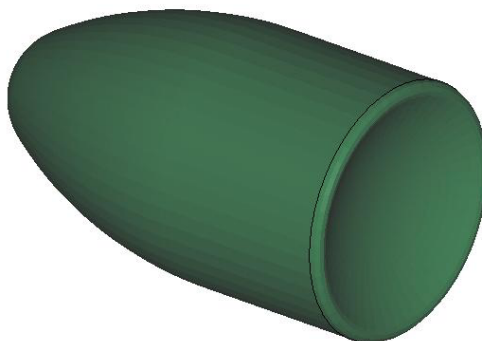
9mm Standart NATO Mermisi



9mm Standart NATO Mermisi



9mm Standart NATO Mermisi



9mm Standart NATO Mermisi

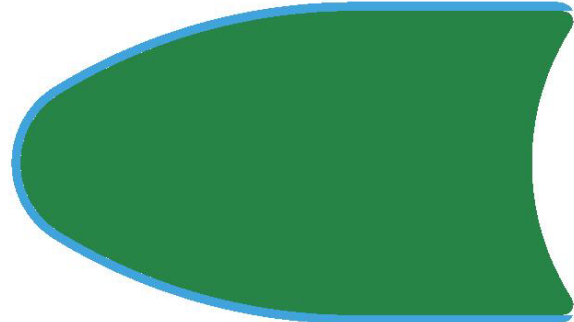


Figure 11. CAD Model of the Bullet

Numerical Model

For the shell element mesh, as it is mentioned before, a very fine mapped mesh is generated inside the target geometry with quadrilateral shell elements. The mesh gets coarser in radial direction to the end. For the research, different element algorithms such as Lagrangian, Eulerian and ALE are investigated preserving the same mesh pattern. For the Lagrangian elements also the effect of number of integration points are also investigated. Two models generated for this purpose, which are single point integration Belytschko-Tsay #2 and fully integrated shell element #16. The mesh topology can be seen in Figure 12. To be consistent between the models solid hexahedral element mesh created with the same pattern but by using three elements through the thickness. The SPH model is also modeled by using the same number of nodes through the thickness with solid elements. A graphical representation of the model for SPH and shell elements can be seen in Figure 13 and 14 respectively.

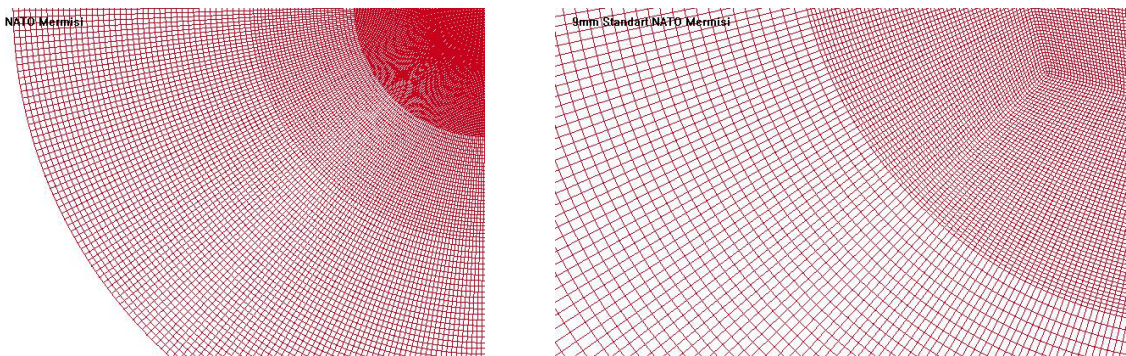


Figure 12. Finite Element Mesh of Target with Shell Element

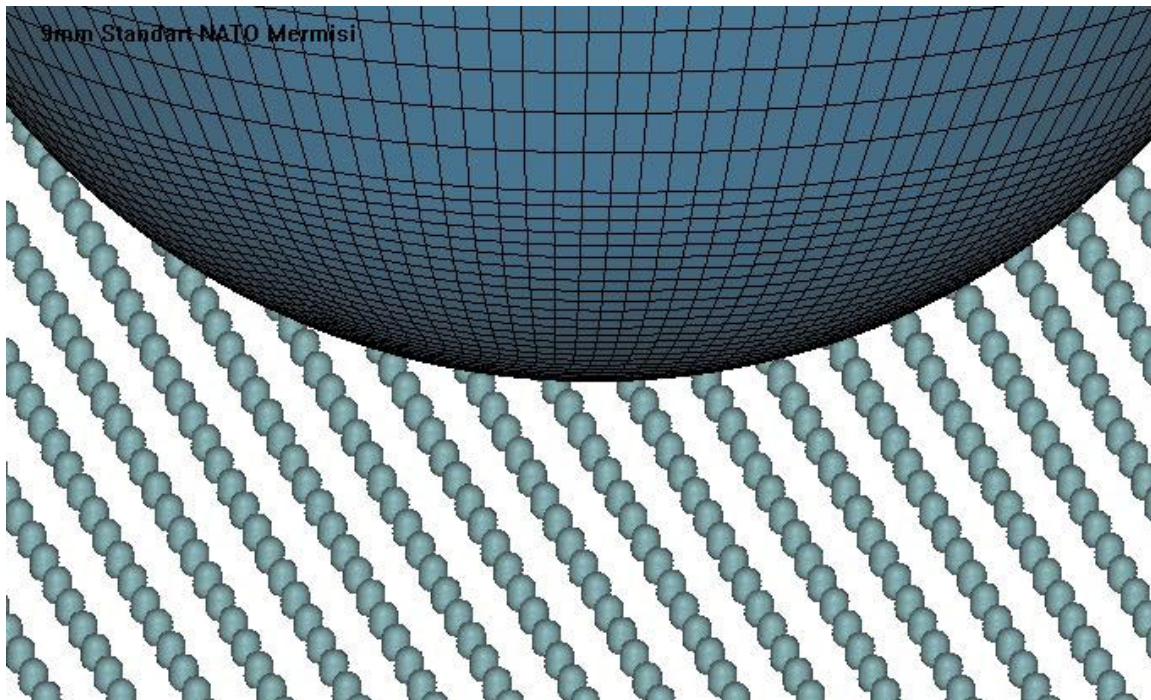


Figure 13. SPH Particles and Bullet

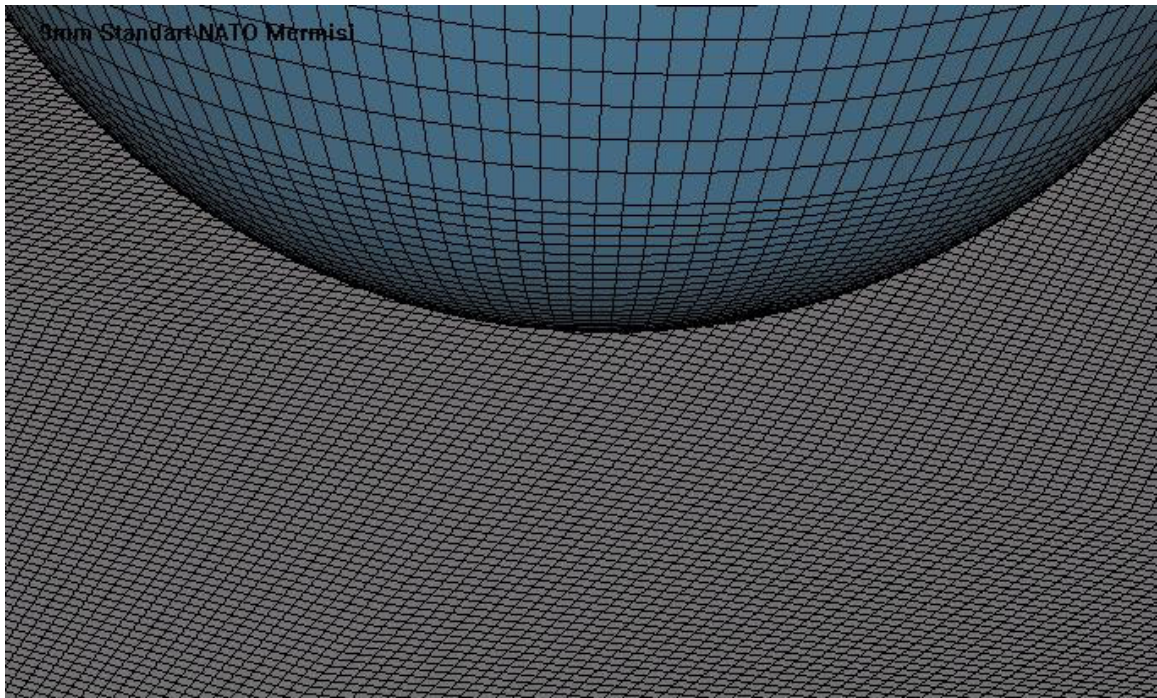
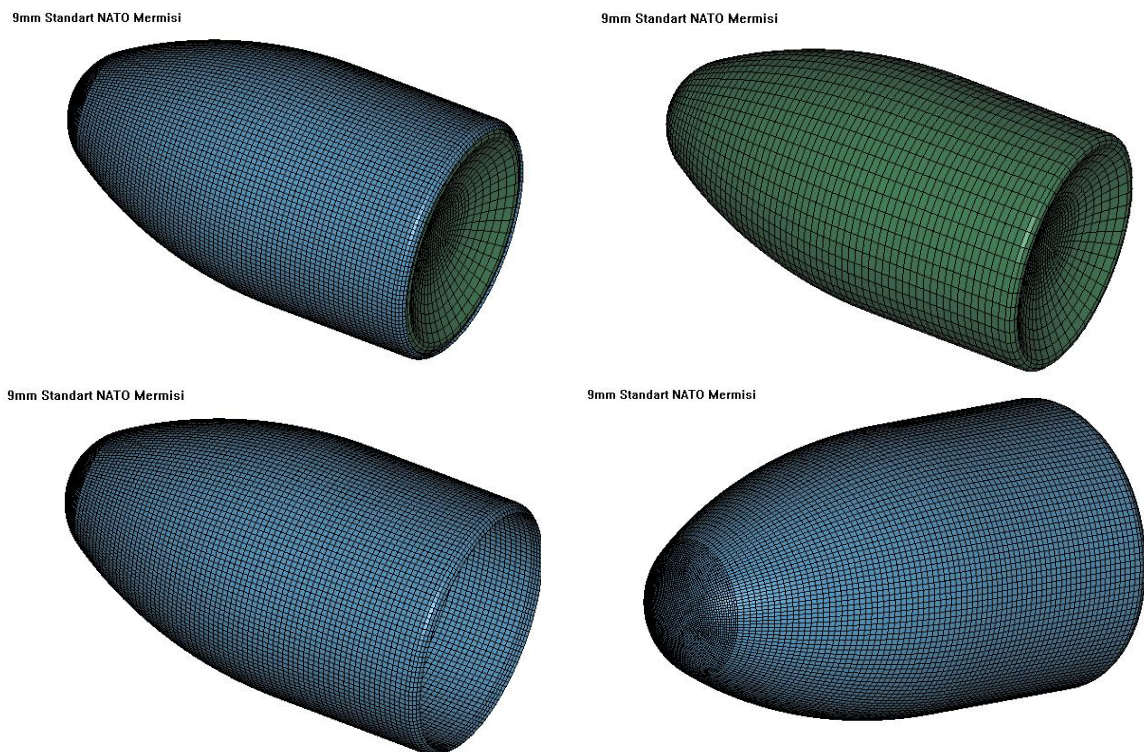


Figure 14. Lagrangian Shell Elements and Bullet

To be again consistent between the models Bullet is modeled by Lagrangian hexahedral elements and used for each case without any changes. Mesh topology and the interface of the core and jacket of the bullet can be seen in Figure 15.



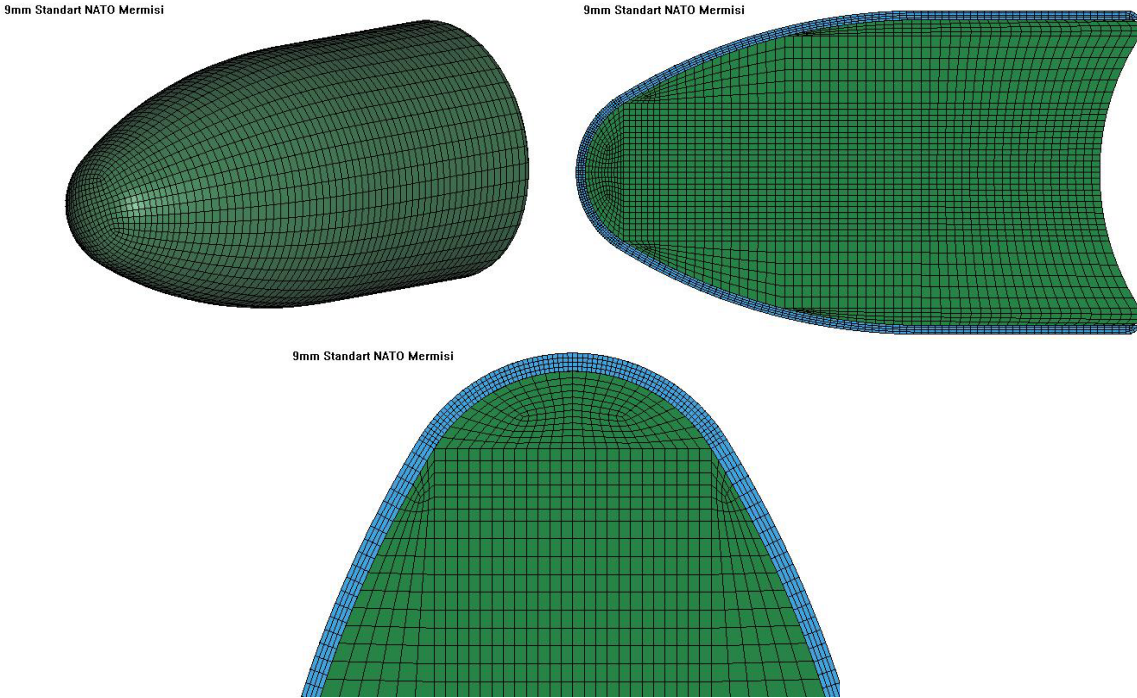


Figure 15. Bullet Mesh

Material Model

Johnson-Cook Material Model

Johnson-Cook material model is used for every particular material to represent the high-speed impact behavior. This model is also supported by an equation of state. Johnson-Cook (JC) is a strain-rate and temperature-dependent (adiabatic assumption) visco-plastic material model. This model is suitable for problems where strain rates vary over a large range, and temperature change due to plastic dissipation causes material softening. The JC model represents the flow stress with an equation of the form [4, 13]:

$$\sigma_y = (A + B\varepsilon^n) \left(1 + C \ln \dot{\varepsilon}^* \right) (1 - T^{*m}) \quad (1)$$

where σ_y is the effective stress, ε is the effective plastic strain, $\dot{\varepsilon}^*$ is the normalized effective plastic strain rate (typically normalized to a strain rate of 1.0 s^{-1}), n is the work hardening exponent and A , B , C , and m are constants. The quantity T^* is defined as:

$$T^* = \frac{T - T_{room}}{T_{melt} - T_{room}} \quad (2)$$

where T_{room} is the room temperature, T_{melt} is the melting temperature and is typically taken as the solidus temperature for an alloy.

Fracture of elements in the JC material model occurs according to the following cumulative damage law:

$$D = \sum \frac{\Delta \varepsilon}{\varepsilon_f} \quad (3)$$

in which

$$\varepsilon_f = [D_1 + D_2 \exp(D_3 \sigma^*)] \left[1 + D_4 \ln \dot{\varepsilon}^* \right] [1 + D_5 T^*] \quad (4)$$

where $\Delta \varepsilon$ is the increment of effective plastic strain during an increment in loading and σ^* is the mean stress normalized by the effective stress. The parameters D_1 , D_2 , D_3 , D_4 and D_5 are fracture constants. Failure of elements is assumed to occur when $D = 1$. The failure strain ε_f and thus the accumulation of damage is a function of mean stress, strain rate, and temperature. Failed elements are removed from the calculation in the progress of the impact analysis.

Mie-Gruneisen equation of state

Mie-Gruneisen equation of state model in this study is used in conjunction with JC material model. It defines the pressure volume relationship in one of two ways, depending on whether the material is compressed or expanded. The Mie-Gruneisen equation of state with cubic shock velocity-particle velocity defines pressure for compressed materials as [9]:

$$p = \frac{\rho_0 C_{sp}^2 \mu \left[1 + \left(1 - \frac{\gamma_0}{2} \right) \mu - \frac{a}{2} \mu^2 \right]}{\left[1 - (S_1 - 1) \mu - S_2 \frac{\mu^2}{\mu + 1} - S_3 \frac{\mu^3}{(\mu + 1)^2} \right]} + (\gamma_0 + a\mu) E_{int} \quad (5)$$

and for expanded materials as:

$$p = \rho_0 C_{sp}^2 \mu + (\gamma_0 + a\mu) E_{int} \quad (6)$$

where E_{int} is internal energy, C_{sp} is the intercept of the vs-vp curve; S_1 - S_3 are the coefficients of the slope of the vs-vp curve, γ_0 is the Gruneisen gamma, a is the first order volume correction to γ_0 , and μ is given as:

$$\mu = \frac{\rho}{\rho_0} - 1 \quad (7)$$

The materials used for the experiment are OFHC Copper, Bullet Lead and Cartridge Brass as target, core and jacket material respectively. The bullet lead is made of Lead alloyed with Antimony. JC and Mie-Gruneisen equation of state model constants for these materials can be found in several resources [13].

Results and Comparison

The possible deformation patterns are summarized in Figure 16 [13]. Since, the thickness of the target foil is 50 μm ; we already can estimate a dishing and petalling formation as a result.

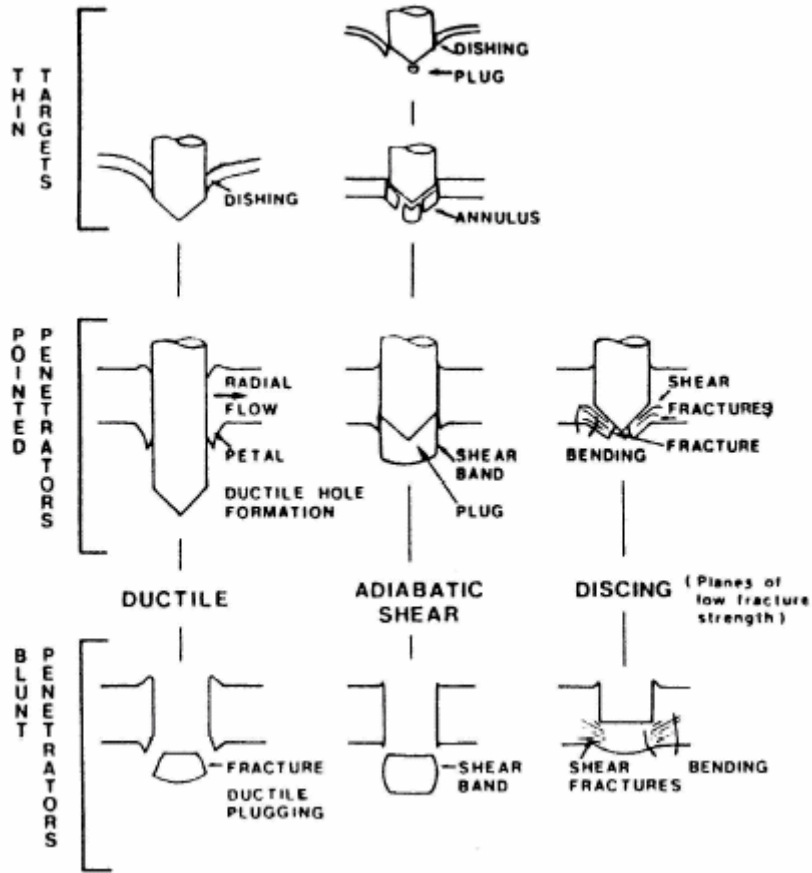
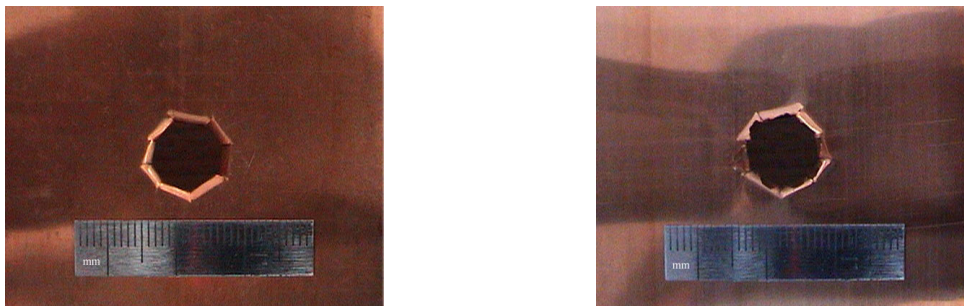
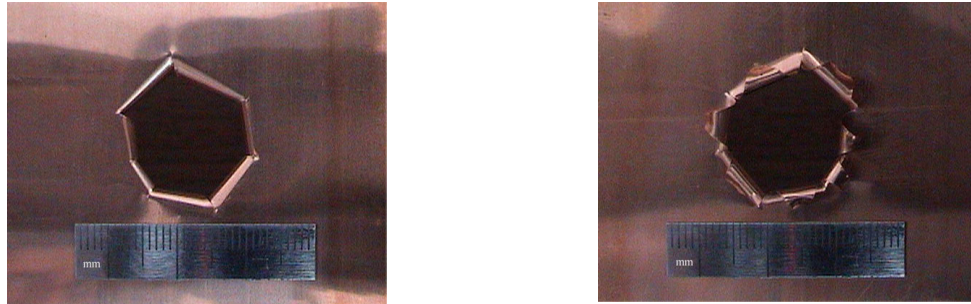


Figure 16. Deformation Patterns

For the 308 mg of gun powder and measured speed of 299.9 m/s, experimentally obtained deformation pattern at the 50 μm foil is as shown in Figure 17. Figure 17 (a) and (b) shows the front and the back view of the first and the second try respectively.



(a) Back and front view of the first try



(b) Back and front view of the second try
 Figure 17. Experimental Results for 299.9 m/s

The following Figures (18-23) represent the numerically obtained results by LS-DYNA for initial impact velocity of 299.9 m/s.

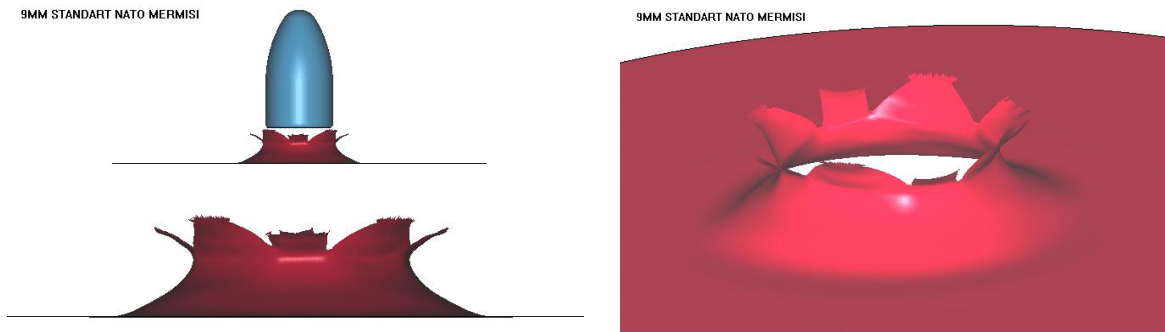


Figure 18. Lagrangian Single Point Integration Belytschko-Tsay Shell Element Results

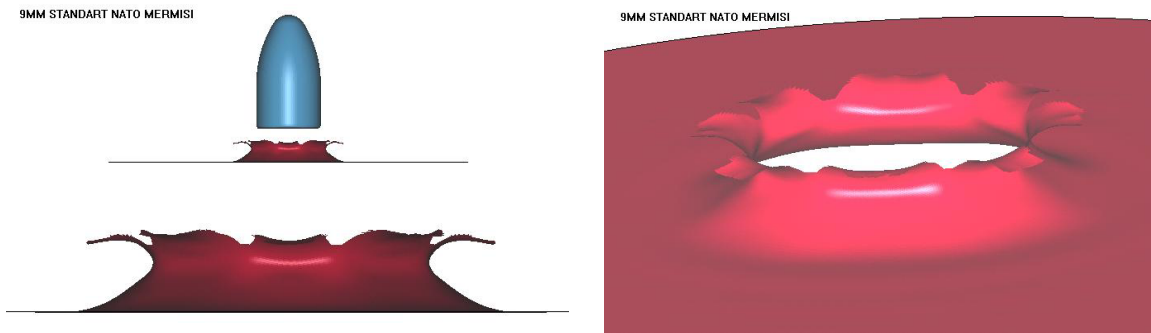


Figure 19. Lagrangian Fully Integrated Shell Element Results

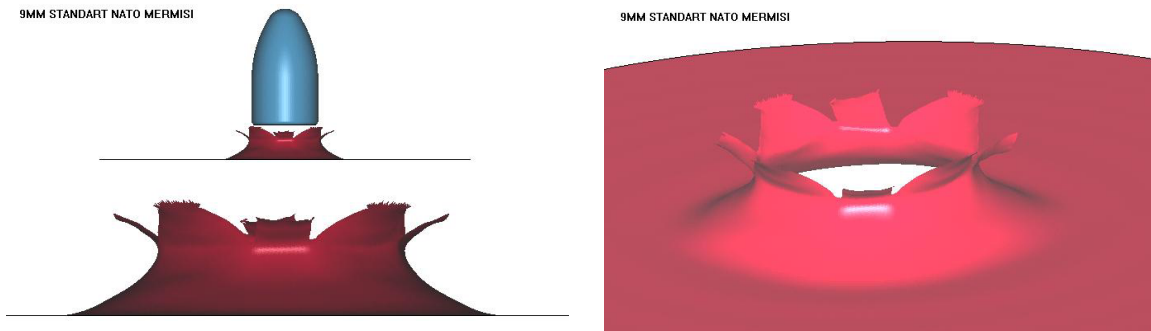


Figure 20. Eulerian Shell Element Results

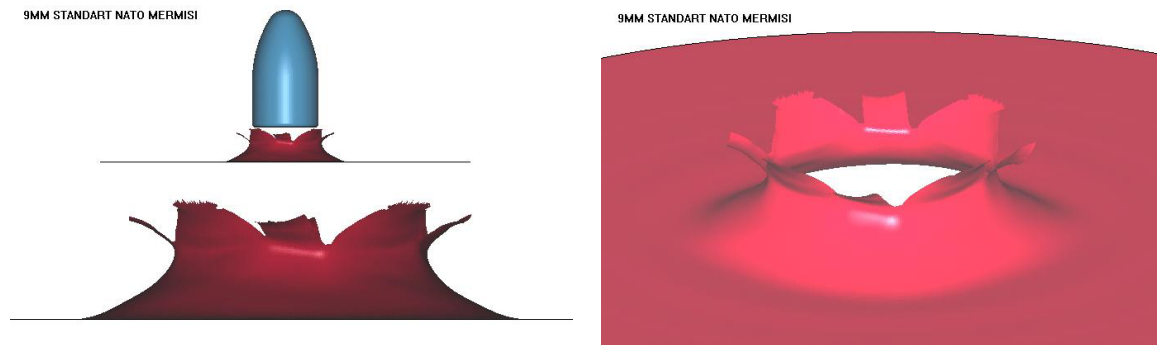


Figure 21. ALE Shell Element Results

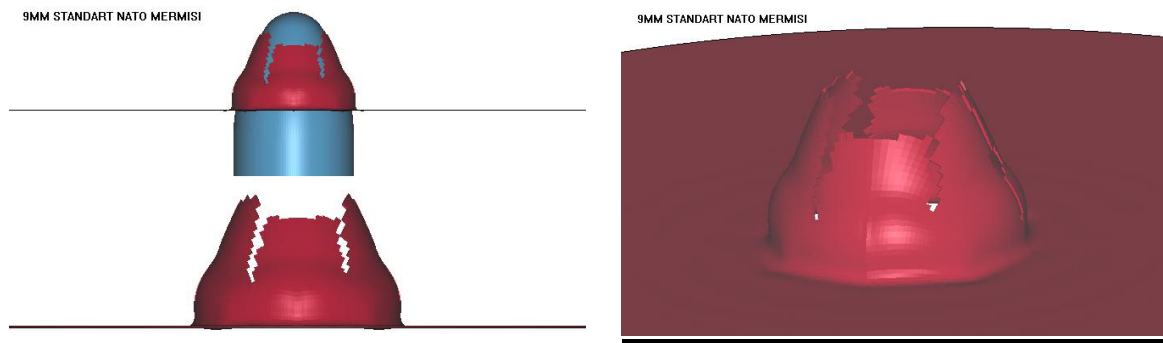


Figure 22. Lagrangian Solid Element Results

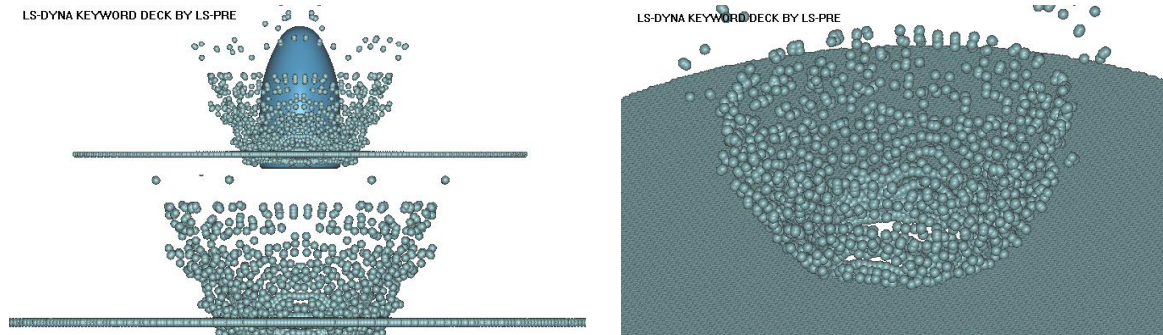
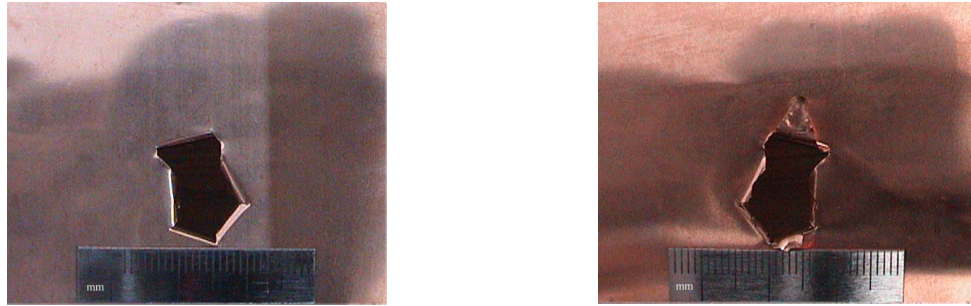
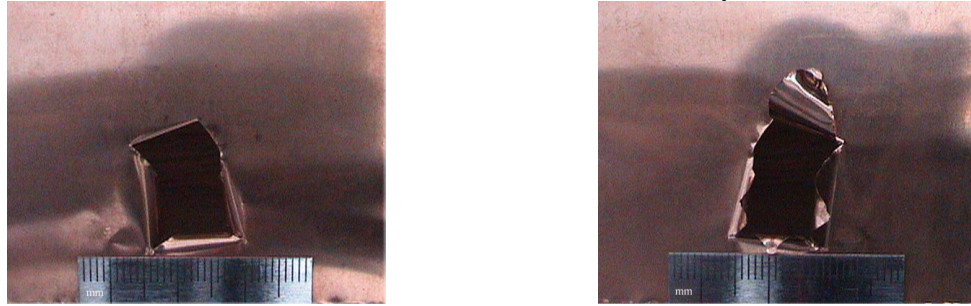


Figure 23. SPH Results

For the 190 mg of gun powder and measured speed of 136.9 m/s, experimentally obtained deformation pattern at the 50 μ m foil is as shown in Figure 24. Figure 24 (a) and (b) shows the front and the back view of the first and the second try respectively.



(a) Back and front view of the first try



(b) Back and front view of the second try

Figure 24. Experimental Results for 136.9 m/s

The following Figures (25-26) represent the numerically obtained results by LS-DYNA for initial impact velocity of 136.9 m/s.

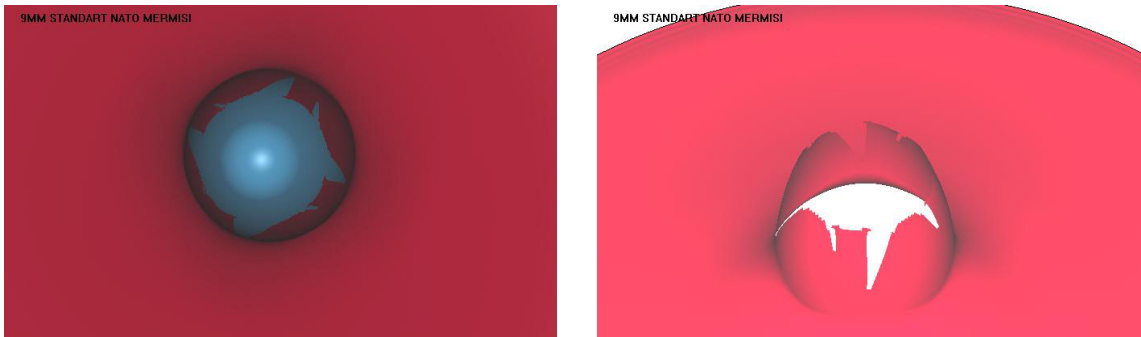


Figure 25. Lagrangian Fully Integrated Shell Element Results

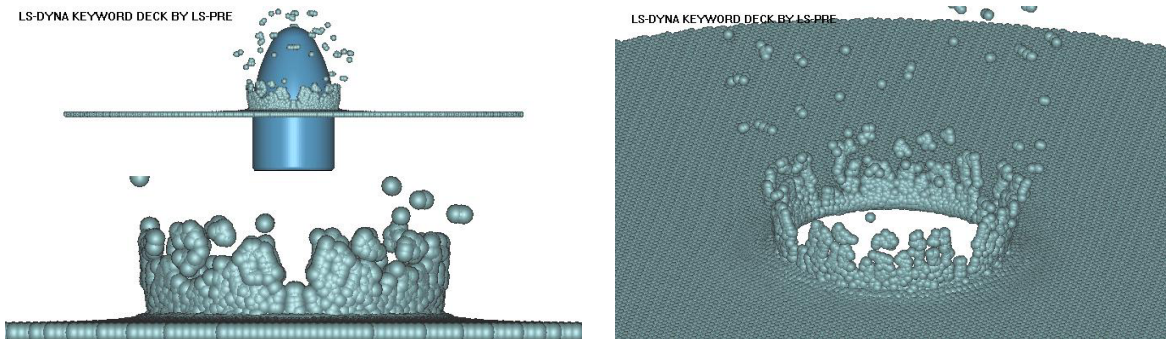


Figure 26. SPH Results

Concluding Remarks

Both the experimental and numerical studies proved a petalling formation at the specs. It is observed that the number of petalling is changing with the speed of impact, the number of petals increases and turns into polygons with irregular edges. This behavior also obtained and validated by numerical studies. For the thin shell structures the best response obtained from fully integrated Lagrangian shell elements, where almost all of the other methods also gave reasonable and acceptable results. Difficulties are seen for the hexahedral solid elements because of the necessary aspect ratio violation, however the results for these elements were also found acceptable. SPH results found to be the same in behavior however, differ in magnitude. It is seen that this method is not as successful as it is in representing the large deformation behaviors in bulk materials. As a future work of this study, also EFG method will be used to compare with the experimental results.

References

1. David L. Littlefield, "The use of r-adaptivity with local, intermittent remesh for modeling hypervelocity impact and penetration", *International Journal of Impact Engineering* 26 433-442, 2001.
2. Iain H.G. Livingstone, Koos Verolme and Colin J. Hayhurst, "Predicting the fragmentation onset velocity for different metallic projectiles using numerical simulations", *International Journal of Impact Engineering*, 26, 453-464, 2001.
3. Naury K. Birnbaum, Nigel J. Francis, Bence I. Gerber, "Coupled techniques for the simulation of fluid-structure and impact problems", <http://www.centurydynamics.co.uk>.
4. Hallquist, J. O., "LS-DYNA Theoretical Manual", Livermore Software Technology Corporation, Livermore, CA, USA, 1997.
5. J.A. Zukas, D.R. Scheffler, "Impact effects in multilayered plates", *Int. J. Solids and Struct.*, 38, 3321-3328, 2001.
6. H. Mahfuz, Y. Zhu, A. Haque, A. Abutalib, U. Vaidya, S. Jeelani, B. Gama, J. Gillespie, B. Fink, "Investigation of high-velocity impact on integral armor using finite element method", *Int. J. Impact Eng.*, 24, 203-217, 2000.
7. T. Borvik, O.S. Hopperstad, T. Berstad, M. Langseth, "A computational model of viscoplasticity and ductile damage for impact and penetration", *Eur. J. Mech. A/Solids*, 20, 685-712, 2001.
8. B.A. Gama, T.A. Bogetti, B.K. Fink, C.J. Yu, T.D. Claar, H.H. Eifert, J.W. Gillespie Jr., "Aluminum foam integral armor: a new dimension in armor design", *Composite Struct.*, 24, 381-395, 2001.
9. Kurtaran H., Buyuk M., Eskandarian A., "Design Automation of a Laminated Armor for Best Impact Performance Using Approximate Optimization Method", *Int. Journal of Impact Engineering*, 29, 397-406, 2003.
10. T. Borvik, M. Langseth, O.S. Hopperstad, K.A. Malo, "Ballistic penetration of steel plates", *Int. J. Impact Eng.*, 22, 855-886, 1999.
11. T. Borvik, O.S. Hopperstad, T. Berstad, M. Langseth, "Perforation of 12 mm thick steel plates by 20 mm diameter projectiles with flat, hemispherical and conical noses Part II: Numerical simulations", *Int. J. Impact Eng.*, 27, 37-64, 2002.
12. Kurtaran H., Buyuk M., Eskandarian A., "Ballistic Impact Simulation of GT Model Vehicle Door Using Finite Element Method", *Theoretical and Applied Fracture Mechanics*, 40, 113-121, 2003.
13. J.A. Zukas, "High Velocity Impact Dynamics", John Wiley & Sons Inc., NY, 1990.